Carbon 170 (2020) 621–629

Contents lists available at ScienceDirect

Carbon

journal homepage: www.elsevier.com/locate/carbon

Research Article

Fundamental understanding on low-friction mechanisms at amorphous carbon interface from reactive molecular dynamics simulation

Xiaowei Li [a, b, c, *], Aiying Wang [c, ***], Kwang-Ryeol Lee [a, **]

[a] Computational Science Center, Korea Institute of Science and Technology, Seoul, 136-791, Republic of Korea
[b] School of Materials and Physics, China University of Mining and Technology, Xuzhou, 221116, PR China
[c] Key Laboratory of Marine Materials and Related Technologies, Zhejiang Key Laboratory of Marine Materials and Protective Technologies, Ningbo Institute of Materials Technology and Engineering, Chinese Academy of Sciences, Ningbo, 315201, PR China

ARTICLE INFO

Article history:
Received 20 May 2020
Received in revised form
21 July 2020
Accepted 7 August 2020
Available online 27 August 2020

Keywords:
Friction mechanism
Graphitization
Passivation
Amorphous carbon
Reactive molecular dynamics

ABSTRACT

Amorphous carbon (a-C) film arouses enormous interest in both scientific and engineering communities because of its excellent anti-friction property. However, due to the complexity of working conditions and the lack of in-situ characterization technique into sliding interface, the direct comparison between two widely accepted low-friction postulations, including the graphitization and passivation mechanisms, has never been performed experimentally. Herein, using reactive molecular dynamics simulation, we comparatively investigated the friction property and structural information of contacting interface under different passivated or graphitized states. For the passivation mechanism, the low friction behavior attributes to the reduction of both the real contact area and shearing strength of sliding interface due to the passivation of a-C dangling bonds. This is different from the graphitization mechanism, which improves the friction property by decreasing the shearing strength only. However, the graphitization mechanism strongly depends on the size and layer number of graphitized structure, causing the transition of sliding interface from a-C/a-C, a-C/G to G/G, which is followed by the low-friction mechanism evolved from passivation, synergistic effect between graphitization and passivation to graphitization mechanism. These disclose the fundamental understanding of friction-reducing mechanism and guide the design of a-C films and the development of related technologies for tribological applications.

1. Introduction

Amorphous carbon (a-C) film is a big family of amorphous carbon structures, composed of sp^3, sp^2, and sp hybridized bonds [1,2]. According to the hybridized structure, a-C can be divided to the graphite-like carbon (GLC) or tetrahedral a-C (ta-C) films, but it also can be divided into a-C and a-C:H films according to the chemical composition [3]. Due to the variable hybridized structure (ranged from graphite to diamond) and composition (C, H, and metal dopants) [3], this endows a-C films with the ability to tailor their mechanical and tribological properties in wide range. In particular, the excellent tribological property makes a-C film being a strong candidate as a protective coating of key components against friction and wear failure, such as automobile engine [4], cutting tools [5], artificial joints [6], space-based technology [7], and micro-electromechanical systems [8,9].

Two popular low-friction mechanisms of a-C films were suggested: the structural graphitization via sp^3-to-sp^2 transformation [10–13] and the passivation of dangling bonds by the chemical termination [14–17] or rehybridization [18–20]. However, due to the difference in working conditions (sliding velocity, normal load, temperature, atmosphere, and mated materials) [16,17,19–22] and the complexity of a-C structures (a-C, a-C:H, ta-C, GLC, roughness, surface state et al.) [1,3,17,20], the direct comparison between the passivation and graphitization mechanisms is not accessible for

* Corresponding author. Computational Science Center, Korea Institute of Science and Technology, Seoul, 136-791, Republic of Korea.
** Corresponding author. Computational Science Center, Korea Institute of Science and Technology, Seoul, 136-791, Republic of Korea.
*** Corresponding author. Ningbo Institute of Materials Technology and Engineering, Chinese Academy of Sciences, Ningbo, 315201, PR China.
E-mail addresses: lixw0826@gmail.com (X. Li), aywang@nimte.ac.cn (A. Wang), krlee@kist.re.kr (K.-R. Lee).

https://doi.org/10.1016/j.carbon.2020.08.014
0008-6223/

experimental approach. This leads to the unavoidable confusion of mechanism governing the low-friction behavior of a-C film. Especially, the spatially resolved structural information of contacting surface, including the quantification of passivated state, real contact area, and the formation of the interfacial nanostructure, is buried because of the lack of in-situ characterization technique into the sliding interface [15]. In addition, whether the presence of graphitic structure at the friction interface ensures the graphitization mechanism is not well comprehended. Even less is known about whether the low-friction behavior of a-C is dominated by the single component or synergistic effect of two above-mentioned mechanisms. These are prerequisite to provide the most reliable explanation for the low-friction process of a-C film in the experiment and promote the development of anti-friction technology for the application.

In the present work, using reactive force field molecular dynamics (RMD) simulation, we designed the different self-mated a-C friction systems, in which the hydrogenated modification of a-C and the addition of graphite-like structure (G) were applied into the system to represent the passivated, graphitized, and co-existed passivated/graphitized interfaces, respectively. For comparison, the interfacial graphitization was also additionally simulated by the pre-annealing treatment of a-C surface. The friction responses of all systems were comparatively investigated. The insight into the information of interfacial structure was carried out to explore the role of graphitization and passivation on the low friction, and the intrinsic characteristics of the above-mentioned two mechanisms were summarized and discussed.

2. Computational details

All calculations, including the preparation of a-C/a-C friction systems with different passivated/graphitized states and their friction simulations, were employed by Large-scale Atomic/Molecular Massively Parallel Simulator (LAMMPS) code [23]. Fig. 1a and d showed the models of self-mated a-C/a-C friction systems used in the present work. Hydrogenation modification of a-C surface was undertaken to fabricate the model of passivated condition. Due to the limitation of short MD simulation time and the strong sensitivity of graphitization to friction parameters (temperature, normal force, sliding velocity et al.), it was difficult for MD simulation to produce the 2D layered graphitization structure at the friction interface directly as experiment [9–13], so the graphite-like structure was introduced into the a-C/a-C interface to approximately represent the graphitization condition and this model was similar to the result reported by Ma et al. [10]. The initial a-C structure of 42.9 × 40.4 × 31.0 $Å^3$ (Fig. 1a) was prepared by an atom-by-atom deposition simulation [24] which was composed of 6877 carbon atoms and had an sp^3 fraction of 24 at.%, an sp^2 fraction of 72 at.% and a density of 2.7 g/cm^3. The H-passivated a-C surfaces (a-C@H, Fig. 1b) with different H contents (10.2 at.% to 24.9 at.%) were fabricated by annealing the a-C at 600 K under different high-pressure H_2 gas conditions, and the detailed process could be found in our previous study [25]. According to the number of H atoms at the a-C surface, the H-passivated structures were named as a-C@122H, a-C@247H, and a-C@351H, respectively. In order to fabricate the a-C with interfacial graphitization, the graphite-like (G) fragments were introduced into the interface, as illustrated in Fig. 1c, in which each G fragment was composed of 66 C atoms with sizes of 11.36 × 12.30 $Å^2$, 4 repeat units were used with random distribution, and the separation distance between the G and the lower or upper a-C film was 3 Å. This friction system was named as a-C@G. The friction system (Fig. 1d), including both the passivated a-C surface and G flakes (a-C@H@G), was also constructed by combining the structures from Fig. 1b and c to explore the potential synergistic effect in improving the friction performance. However, the extra pre-annealing approach of a-C surface at 600–3000 K was also performed to achieve the graphitized friction interface, whose result could not only provide a contrast for that obtained using above-mentioned method in Fig. 1c, but also validate the universality in theory developed by this work.

Similar to the previous studies [19,20], a three-layer assumption model was applied to each system, including fixed layer (blue background in Fig. 1a) for simulating the semi-infinite system, thermostatic layer (purple background in Fig. 1a) being maintained at 300 K through the microcanonical ensemble with a Berendsen thermostat [26], and free layer consisted of the remnant atoms in Fig. 1a for modeling the evolution of tribo-induced interfacial structure. Time step was 0.25 fs? Periodic boundary condition was imposed along the *x*- and *y*-directions. ReaxFF potential developed by Tavazza et al. [27] was utilized to accurately describe the *C*–C, *C*–H, and H–H interactions in the whole system, whose reliability has been validated by our previous works [19,28,29].

During the friction process, a three-step process was adopted: (i) geometric optimization at 300 K for 2.5 ps; (ii) loading process to achieve the specified value of contact pressure (5 GPa) during 25 ps; (iii) sliding process with fixed contact pressure and sliding velocity (10 m/s) along the *x*-direction for 1250 ps? Our [19,25,28,29] and previous studies [10,20,30,31] have already confirmed that the high contact pressure (5 GPa) was appropriate to examine the friction behavior on an atomic scale. In addition, due to the limitation of short MD simulation time and computational resources, the high sliding velocity was necessary to simulate a long sliding distance and sufficiently sample phase space. Moseler et al. [30] also indicated that when the sliding velocity was below the speed of sound in materials, reliable modeling of the shear response of materials could be obtained because of the sufficient dissipation of heat generated in contact during sliding. After the friction process, the forces from the *x* and *z* directions of the fixed layer of bottom a-C substrate were counted as friction force, *f*, and normal force, *W*, respectively, for each case; the real contact area, *A*, was calculated according to Hertzian theory:

$$A = \frac{W}{\sigma} \tag{1}$$

where σ was Hertzian contact pressure, being a constant value of 5 GPa in this work.

3. Results and discussion

According to the evolution of friction and normal forces with sliding time (Fig. S1 of Supplementary Data), the friction results are evaluated for each case using the values from the last 200 ps of the stable sliding stage, as shown in Fig. 1e and Fig. S2a of Supplementary Data. It can be observed that when all systems work under the same contact pressure, there is a slight difference in the normal force value (Fig. S2a of Supplementary Data), attributing to the change of real contact area at the sliding interface, as will be discussed later. For the self-mated pure a-C system [29], the existence of a large number of dangling bonds promotes the strong chemical bonding between the mated a-C surfaces following the high friction force (Fig. 1e) and obvious running-in process. This is in consistence with Harrison's reports [17,20]. In the a-C@G system, after introducing the small G flakes into the interface, the high friction force is also obtained, similar to pure a-C case. This suggests that the anti-friction behavior of a-C, contributed by the interfacial graphitization in the experiments [9,12,13], may be strongly dependent on the size and layer of graphitized structure, as will be discussed later.

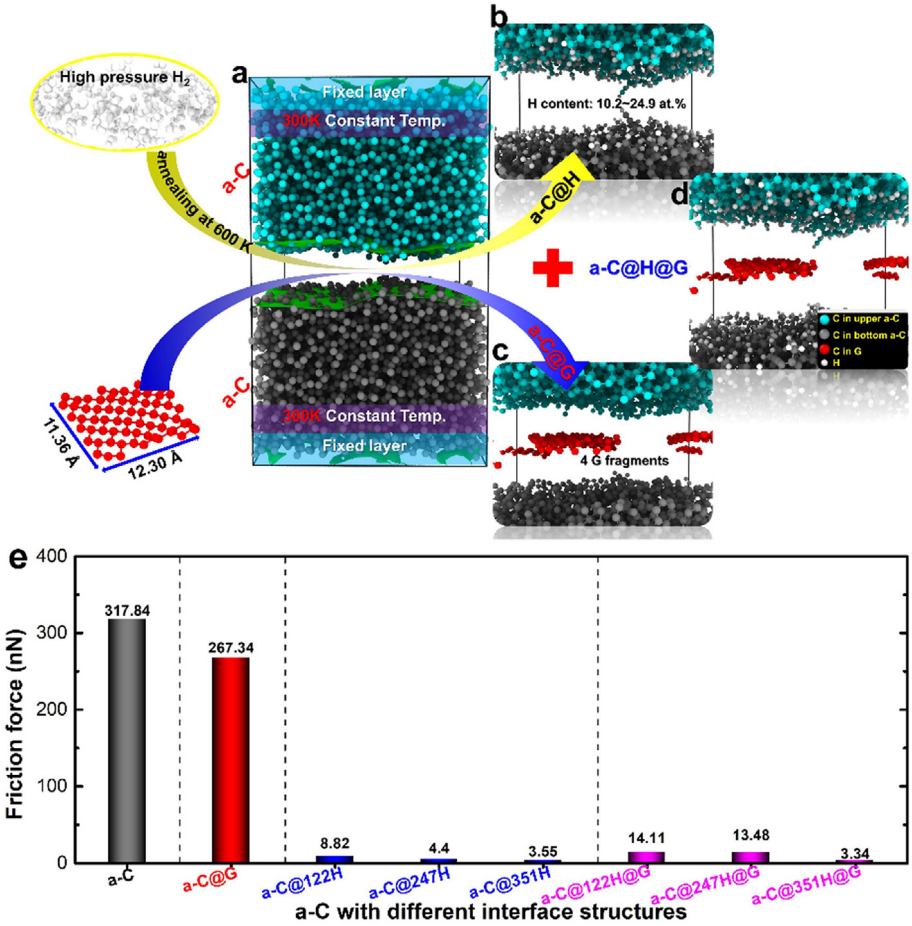

Fig. 1. Simulated models and friction results of self-mated friction systems. (a) Model for pure a-C; (b) Model for a-C@H, in which the H-passivated structures are named as a-C@122H, a-C@247H, and a-C@351H, respectively, according to the number of H atoms at the a-C surface; (c) Model for a-C@G, in which 4 repeat G fragments composed of 66 C atoms in each unit are included; (d) Model for a-C@H@G friction system consisted of different passivated a-C surfaces and G flakes. (e) Friction force values of self-mated pure a-C, a-C@G, a-C@H, and a-C@H@G systems. (A colour version of this figure can be viewed online.)

However, when the a-C surface is passivated by H to form the self-mated a-C@H system, the friction force is drastically reduced, and it further decreases with increasing the surface H content from 10.2 to 24.9 at.% [25]. Compared to the pure a-C, the friction force in a-C@351H decreases by 99%, indicating the significant role of passivation mechanism on the improvement of friction behavior, which is consistent with previous simulations [11,17,20] and experiments [32,33]. Especially for the a-C@H@G system, both the passivation and graphitization of interface are considered simultaneously at the sliding interface. Although it shows a serious reduction of friction force compared to the a-C and a-C@G cases, the existence of G flakes prompts the friction force to increase rather than decrease by comparing with the a-C@H system. This implies that the small G flake cannot play a synergistic effect with surface passivation to enhance the anti-friction property. In addition, it further confirms that the graphitization mechanism should be dominated by the specified G structure if it works on the low-friction behavior of a-C film in the experiment, as will be discussed later.

Moreover, the temperature rise at the sliding interfaces of a-C and a-C@G systems is also higher than those in a-C@H and a-C@H@G systems, as given in Fig. S2b of Supplementary Data. The flash temperature between both surface asperities can be estimated as following [16,34]:

$$\Delta T = \frac{\mu W v}{8 a K_{a-C}} \tag{2}$$

where ΔT is the rise of the flash temperature at the contact between the asperities; μ, W, and v are the friction coefficient, applied normal force, and sliding velocity, respectively; a is the radius of the real contact area, and $K_{a\text{-}C}$ is the thermal conductivity of the a-C material. Hence, the change of flash temperature attributes to the difference in friction force induced by mechano-chemical interactions at the sliding interface.

Friction behavior is closely related to the surface/interface structure during the friction process [15]. In order to disclose the insight on the friction mechanism under different passivated and/or graphitized conditions, the interfacial region, in which the mechano-chemical interaction occurs during the sliding process, needs to be defined first for each case. According to the distributions of C (from both the a-C and/or G) and/or H atoms along the relative position from the bottom of system, the interfacial widths are obtained for all systems, as illustrated in the regions with the gray background of Fig. 2 and Fig. S3 of Supplementary Data. It is clearly observed that due to the relatively low contact pressure, the friction-induced structure transformation mainly occurs at the interfacial region, consistent with previous reports [19,25]. Then, the interaction between the mated materials under the presence of

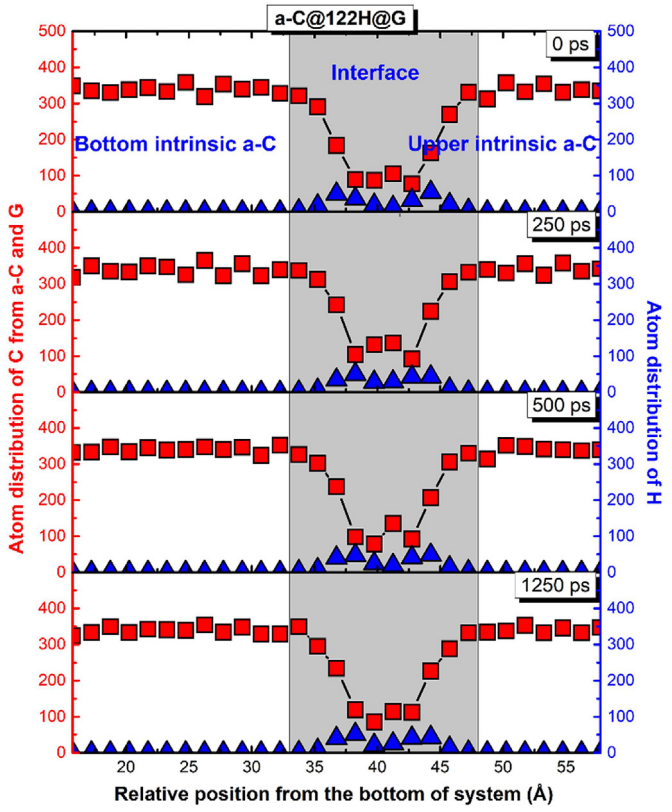

Fig. 2. Atomic distributions of C (from both the a-C and G) and H atoms along the relative position from the bottom of a-C@122H@G system during the sliding process. (A colour version of this figure can be viewed online.)

surface passivation and/or graphitization and the friction-induced evolution of interfacial structure are analyzed.

Fig. 3a and d display the morphologies of sliding interfaces before and after sliding processes for each case. It can be found that for the pure a-C friction system (Fig. 3a), due to the large amount of dangling bonds at the sliding interface (sp-C fraction-21.0 at.% and 1-coordinated C fraction-1.8 at.%), the self-mated a-C surfaces interact in the form of covalent bonding, leading to the reconstruction of sliding interface [29]. Although this reconstruction process facilitates the reduction of both the sp-C and 1-coordinated C fractions (Fig. 3e), the strong interfilm interaction prohibits the shearing motion of mated materials following the high friction force (Fig. 1e). In addition, the transition of sp^3-C to sp^2-C during sliding process attributes to the tribo-induced breaking of stressed bonds reported by Moseler et al. [35].

In the a-C@G system, the small G flakes are introduced into the sliding interface. During the friction process, the side C atoms of G tend to bond with the dangling bonds of both the mated a-C surfaces (Fig. 3b). Combined with the shearing effect, these lead to the complete dissociation of G flakes, which cannot play a positive role to reduce the friction force (Fig. 1e). Therefore, the changes of both the friction force and interfacial structure are similar to those from the pure a-C case, as shown in Figs. 1e and 3e. In addition, this suggests that the existence of graphitized structure, which is observed at the friction interface in the experiments [9–13], is strongly affected by the dangling bonds of a-C, which is confirmed by the following results of a-C@H@G systems.

Taking the a-C@122H system for example (Fig. 3c and e), compared to the pure a-C system, using H to passivate the a-C surface could not only reduce the fractions of sp-C (12.7 at.%) and 1-coordinated C (0 at.%) dangling bonds of a-C surface, but also effectively prevent the chemical interfilm interaction of self-mated a-C surfaces via the repulsive force of H atoms [36,37], improving the friction property obviously. Especially, the friction force as a function of H content further decreases due to the increased repulsive force values of H atoms, as illustrated in Fig. S4 of Supplementary Data, which has been clarified by our previous study [25].

For a-C@H@G system, both the G structure and passivated a-C surface are introduced, exhibiting different evolution of interfacial structure compared to the a-C@G and a-C@H cases. For example, in a-C@122H@G system, due to the H-induced reduction of a-C dangling bonds, the chemical interaction between the G and a-C surface is weakened and thus the G flakes can exist at the passivated a-C surface during the sliding process without the serious dissociation (Fig. 3d), being different with the a-C@G case. Especially, the structural integrity of graphitized flakes is further improved with enhancing the passivated state of a-C surface (Fig. S5 of Supplementary Data). This indicates that the reduction of a-C dangling bonds, which can be achieved by the chemical termination [11,17,25] or friction-induced structural transformation [19,20,29], is beneficial for the initial formation and growth of graphitized structure at the interface as suggested by previous studies [10,11], although the shear-induced temperature rise during friction process may dominate the graphitization of a-C structure according to *P-T* phase diagram [10]. On the other hand, compared to the a-C@H system, the graphitized structure existed in a-C@H@G system has little effect on the stress state of H atoms and the corresponding repulsion force values, as confirmed by Figs. S4 and S6a of Supplementary Data.

However, due to the addition of small G flakes, the friction force of a-C@122H@G increases to 14.41 nN by comparing with that of the a-C@122H (8.82 nN) (Fig. 1e). This is because the small G flakes crosslink the mated a-C surfaces by the chemical bonding with sp-C atoms of a-C surface rather than smooth the sliding a-C surface, resulting in the indirect interfilm interaction and thus increasing the shearing strength of sliding interface (Fig. 3d). But this G-induced crosslinking interaction can be weakened by further passivating the a-C surface, which decreases the potentially active site of a-C surface to bond with G flakes (Fig. S6b of Supplementary Data). Consequently, when the small graphitized structure is generated at the interface, the observed low-friction behavior in the a-C@H@G system should be dominated by the passivation mechanism of a-C surface rather than the graphitization mechanism.

From the above-mentioned analysis, we mention the effect of interfacial graphitization on low-friction behavior, which is not only dependent on the passivated state, especially sp-C dangling bonds, of a-C surface, but also related with the graphitized structure, such as size and layer number. Many experiments [9,12,13,38,39] also reported the presence of graphitized structure with large-scale and multilayer features, which governed the superlubricity of a-C films. Therefore, when the size and layer number of G flakes are increased, the further atomic-scale understanding on the friction property and corresponding interfacial structure is required to disclose the fundamental low-friction mechanism of a-C film.

Compared with the small G flake (size-11.36 × 12.30 $Å^2$) used in Fig. 1e, the G structures, including the one with middle size of 29.52 × 29.83 $Å^2$ and composed of 363 C atoms (named as G-M) and the other with large size of 40.59 × 39.06 $Å^2$ and composed of 646 C atoms (named as G-L), are fabricated separately and then introduced into the a-C sliding interface (Fig. 4). Moreover, the effect of different G layer numbers on the friction behavior, such as monolayer (named as G-M-1 and G-L-1) and bilayer (named as

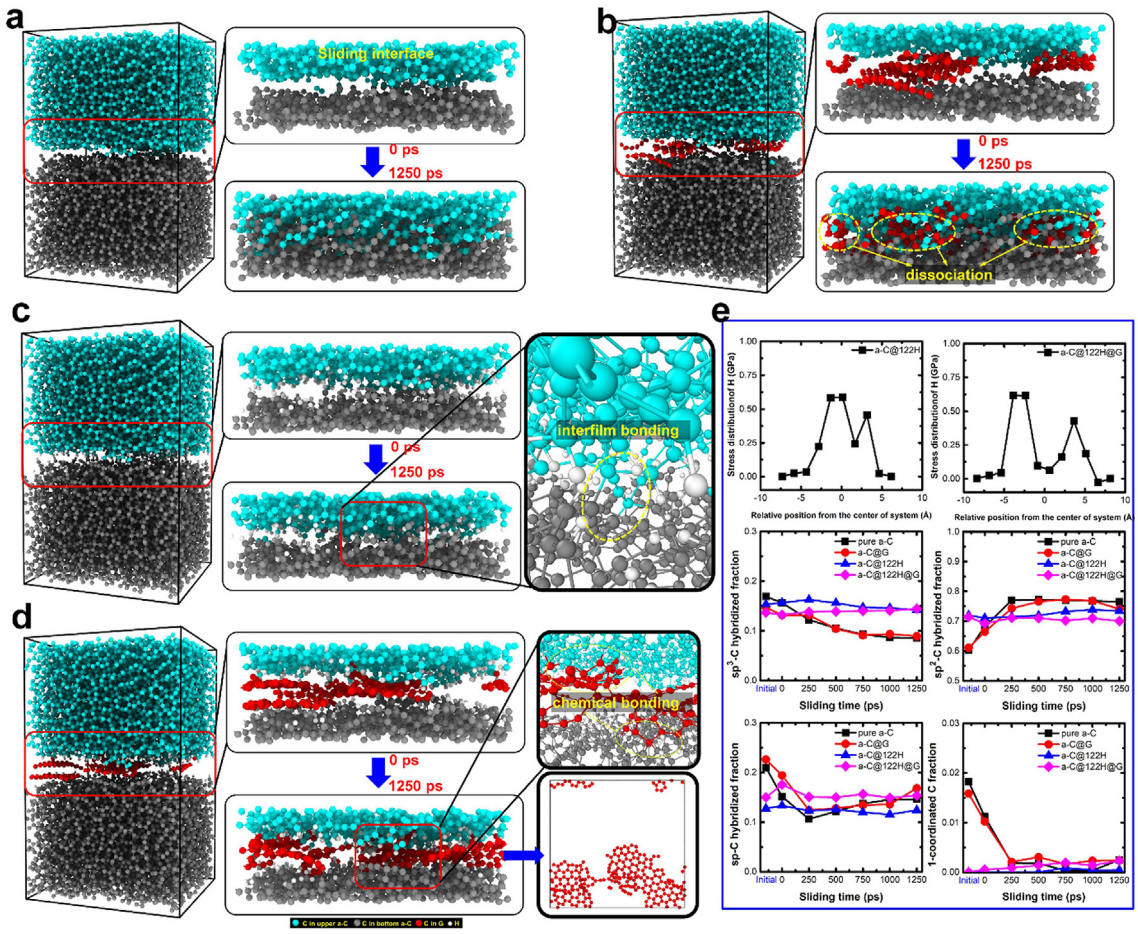

Fig. 3. Morphologies of sliding interfaces before and after sliding processes in self-mated (a) pure a-C, (b) a-C@G, (c) a-C@122H, and (d) a-C@122H@G systems, respectively. (e) Stress distributions of H atoms in a-C@122H and a-C@122H@G systems, and the evolution of interfacial hybridization structure (sp^3-C, sp^2-C, sp-C, and 1-coordinated C) with sliding time for each case. (A colour version of this figure can be viewed online.)

G-M-2 and G-L-2), are also comparatively investigated to explore the dependence of friction property on G multilayer (Fig. 4).

It can be obtained that for the a-C@G-M-1 system, the friction results (Fig. 4a and b) are also similar to the a-C@G case with the serious dissociation of G structure and the reconstruction of the interfacial structure during the sliding process (Fig. 4b and Fig. S7 of Supplementary Data). However, when the G size increases from G-M-1 to G-L-1 (Fig. 4c), the strong interaction between the mated a-C surfaces can be shielded by the G structure following the small change of interfacial hybridized structure (Fig. S7 of Supplementary Data). In particular, the G structure is anchored to one a-C surface by the chemical bonding (Fig. 4c), smoothing the a-C surface [40,41] and also leading to the transition of shearing interface from a-C/a-C to a-C/G (see Supplementary Movie S1), which obviously decreases the friction force to 48.72 nN from 261.10 nN of a-C@G-M-1 system (Fig. 4a).

Supplementary data related to this article can be found at https://doi.org/10.1016/j.carbon.2020.08.014.

Moreover, different friction response can be achieved, when the layer number of the graphitized structure increases from monolayer to bilayer. Compared to the a-C@G-M-1 system, for the a-C@G-M-2 system presented in Fig. 4d, the G side atoms also interact with the a-C surfaces in the form of covalent bonds, which not only passivates the sp-C dangling bonds of a-C surface (Fig. S7 of Supplementary Data), but also brings the slight tribo-induced dissociation of G structure (Fig. 4d). However, due to the bilayer character of G structure, each layer is anchored to the different a-C surfaces, respectively, acting as a solid protective film to smooth the a-C surface and also reduce the interfilm interaction between the mated films. The sliding interface is also transited from a-C/a-C to the synergistic G/G and a-C/G interfaces (see Supplementary Movie S2), accounting for the reduction of friction force (Fig. 4a). Furthermore, as the G-L-2 is present at the a-C/a-C interface (Fig. 4e), its one layer is also stably anchored to the bottom a-C surface and another is bonded with the upper a-C surface. Due to the large size and bilayer characters of G, the mated a-C surfaces are totally covered by the G layer without the interfilm interaction, and thus the friction behavior is fully dominated by the intermolecular interaction of G/G interface (see Supplementary Movie S3). This leads to the ultra-low friction force of 1.12 nN (Fig. 4a), which is much lower than that from any a-C@H system.

Supplementary data related to this article can be found at https://doi.org/10.1016/j.carbon.2020.08.014.

Therefore, based on the above-mentioned analysis, it can be deduced that when the formed graphitized structure at the friction interface is large and thick enough, the low-friction behavior mainly attributes to the graphitization mechanism, even though the a-C surface is passivated by the chemical termination [14–17] or rehybridization [18–20]. However, it should be noted that following the decrease of size and layer number of graphitized structure, the dominated mechanism will be transferred from graphitization-dominated to passivation-dominated mechanism.

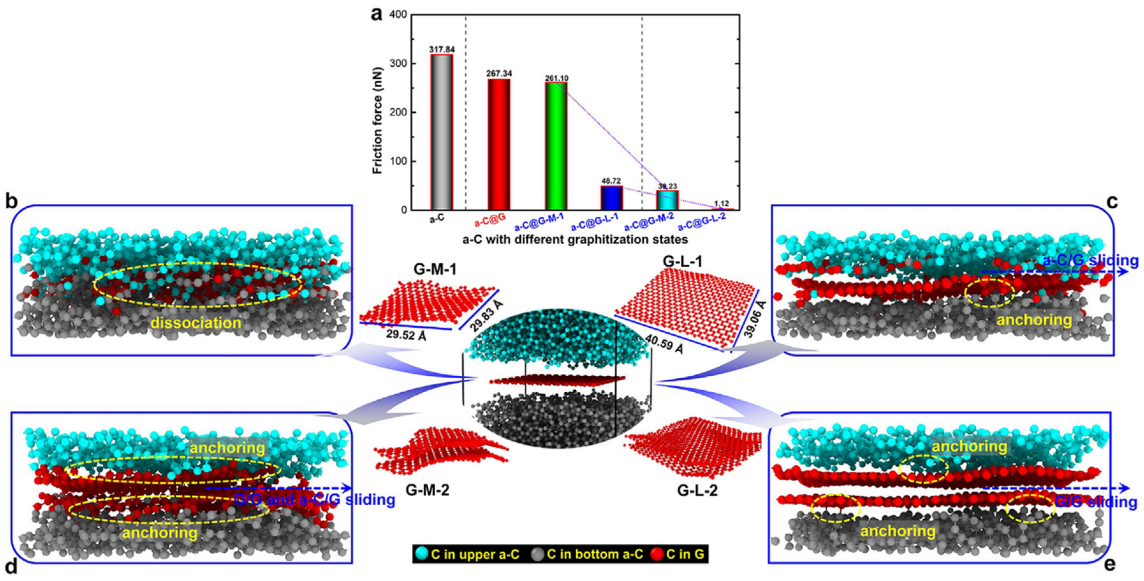

Fig. 4. Friction results of a-C friction systems with different graphitization states, including (a) friction force and final morphologies of interfaces after the sliding processes in (b) a-C@G-M-1, (c) a-C@G-L-1, (d) a-C@G-M-2, and (e) a-C@G-L-2 friction systems. (A colour version of this figure can be viewed online.)

Especially, when the graphitized structure is not large enough, such as the a-C@G-M-2 system in Fig. 4d, there will be partial a-C surface which is not covered by the graphitized structure. In this naked a-C surface region, the passivation of dangling bonds is conductive to reduce the chemical interaction of a-C with the graphitized structure, promote the formation of thick and new graphitized layer, and thus cause the easy sliding of G at the interface, exhibiting a synergistic effect of graphitization and passivation mechanisms on the low-friction property. This is confirmed by the additional calculation of a-C@122H@G-L-1, a-C@122H@G-L-2, and a-C@122H@G-M-2 friction systems, which present lower friction forces than the cases without surface hydrogenated passivation (Fig. S8 of Supplementary Data).

Additionally, these results in Fig. S8 of Supplementary Data also indicate that for the graphitization-dominated friction, the presence of interfacial passivation always facilitates the further reduction of friction force, such as a-C@122H@G-L-1. But for passivation-dominated case, the friction behavior is highly affected by the graphitized structure and the small graphitized structure will result in the additional friction of a-C, such as a-C@122H@G in Fig. 1e. In particular, for these cases with the graphitized structure, the change of friction force with the surface area of existed graphitized structure after the sliding process is also evaluated approximately, as given in Fig. S9 of Supplementary Data. It suggests that only when the surface area of formed graphitized structure is larger than the real contact area of friction interface in pure a-C system, it can make contribution to the low friction behavior of a-C.

Fig. 5a also shows the relationship between the friction force and the real contact area for each case. By comparison with the pure a-C system (875.14 Å^2), note that for the systems applicable to the passivation mechanism, the real contact area after the friction process is smaller than that from pure a-C case, agreeing well with previous experimental [42,43] and simulation [31] works. On the contrary, for the systems applicable to the graphitization-dominated or passivation/graphitization synergistic mechanism, they are normally accompanied by the increase of the real contact area, which is first mentioned in the present work. So the change of the contact area can be treated as a key clue to distinguish the underlying low-friction mechanism combined with the transformation of interfacial structure. However, due to the limitation of experimental technology, characterizing the real contact area in the experiment remains a big challenge until now, which will promote the R & D of new testing technology. In addition, it is well known that the friction force is related to the contact area and shearing strength of sliding interfaces [44], which can be described as following

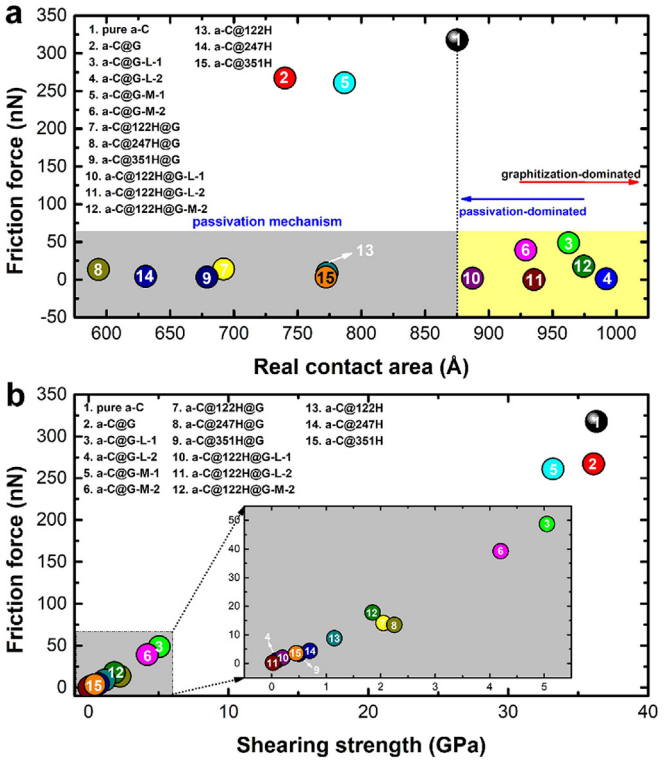

Fig. 5. Relationship between the friction force and (a) the real contact area or (b) shearing strength for each case. (A colour version of this figure can be viewed online.)

$$f = S \times A \quad (3)$$

where S is an effective shearing strength of the mated materials and A is the real contact area at the sliding interface. Fig. 5b illustrates the change of friction force as a function of shearing strength. So Fig. 5a and b reveal that compared with the self-mated pure a-C film, for the graphitization mechanism, the low-friction behavior is achieved by reducing the shearing strength, while for the passivation mechanism, it decreases the friction force by reducing both the real contact area and shearing strength simultaneously.

In addition, in this work the graphitized interface is obtained by the direct addition of graphite-like structure because it is still a big challenge for short MD simulation scale to generate the 2D layered graphitized interface in-situ as experiment. In order to further confirm the graphitization-induced low-friction mechanism as discussed above, the a-C with graphitized surface is produced first by the annealing process at 3000 K using RMD simulation with canonical ensemble and then is adopted to conduct the friction simulation, as shown in Fig. 6a. Note that the annealed system with graphitized surface achieves the stable friction stage quickly without running-in process due to the smooth surface and the absence of sp-C dangling bonds (Fig. 6b). Especially, compared to the initial a-C case, it shows the significant reduction of friction force by 99.75% as shearing strength while followed by the increase of real contact area at the friction interface (Fig. 6c). This ascribes to the weak intermolecular interaction between graphitized layers (see Supplementary Movie S4) and thus there almost has no change in the interfacial structure (Fig. 6c). These results agree well with the above-mentioned analysis in Fig. 5, suggesting that the low-friction mechanism conveyed by this work could be applied to the systems in simulations and experiments.

Supplementary data related to this article can be found at https://doi.org/10.1016/j.carbon.2020.08.014.

Moreover, it should be mentioned that if the graphitization mechanism works for reducing the friction, it is normally accompanied by the increased fraction and structural ordering of sp^2-C phase, even the formation of lamellar structure to achieve the ultralow or superlubricity state. Harrison et al. [17,20] reported that if there was only the increase of sp^2-C fraction, these unsaturated carbon atoms could serve as initiation points for the formation of covalent bonds between the counterface and the film, aggravating the adhesive interactions and thus causing an increase in friction during sliding process. This is also confirmed by our previous simulation [29]. To further highlight the necessity of the ordering or lamellar structure of the sp^2-C phase in graphitization mechanism to reduce the friction, the a-C films with different graphitized degrees, which are fabricated by annealing treatment under different temperatures (600, 1500, and 3000 K), are used to further conduct the friction simulation. The corresponding results are illustrated in Fig. 7. It reveals that compared to the initial case, although the sp^2-C fraction of a-C surface annealed at 600 K increases, the friction force almost has no reduction. However, as the annealing temperature increases to 1500 K, the small graphitic structures are present following the decrease of friction force. Especially, with further increasing the annealing temperature to 3000 K, the graphitized degree of a-C surface is highly improved, accounting for the ultra-low friction force value. Therefore, these previous [17,20,29] and present results confirm that for the graphitization mechanism, except the increased sp^2-C fraction, the ordering or even the lamellar structure of the sp^2-C phase is requisite to achieve the low-friction behavior. However, although Luo et al. [15] successfully observed the presence of graphitized structure at friction interface using the most advanced STEM and EELS approach, it was still intractable to extract the information of interested region in situ, especially at the very thin friction contacting interface, due to the complexity of a-C structure, low fraction and size of graphitic flakes, and the limitation of characterization techniques.

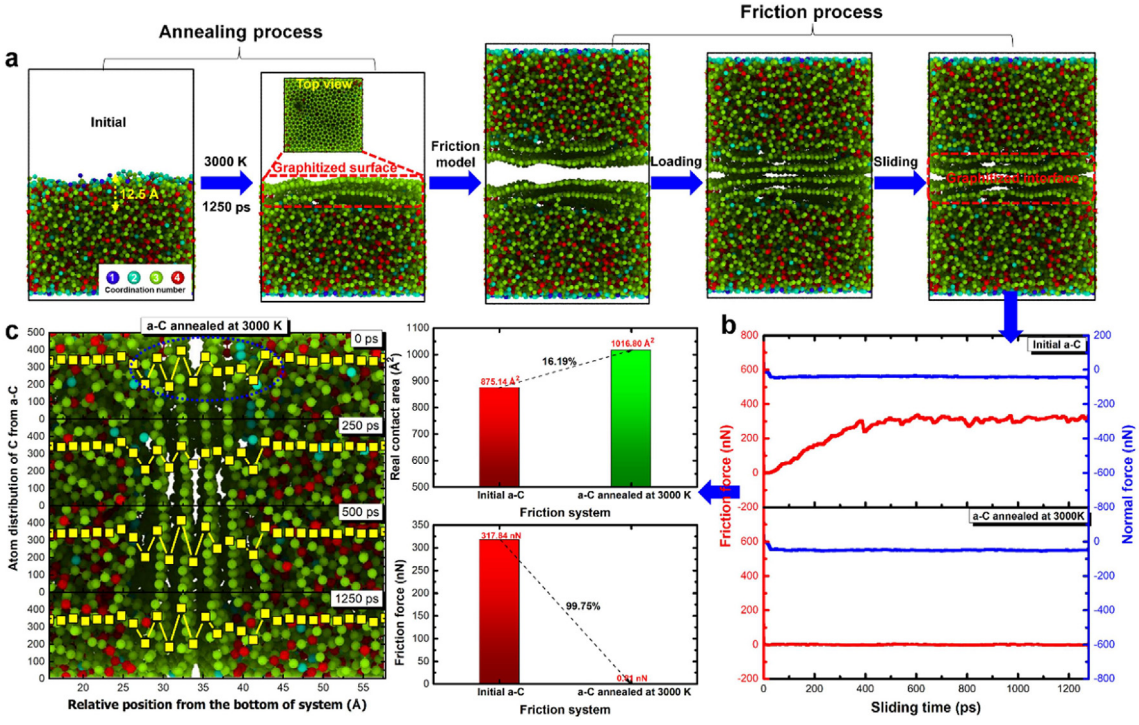

Fig. 6. Friction results of a-C with graphitized surface by annealing process. (a) Annealing process at 3000 K to fabricate the a-C with graphitized surface and friction simulation. (b) Friction curves for the systems using initial a-C and annealed a-C, respectively. (c) Friction results including friction force, real contact area, and atom distribution of C atoms in the system with annealed a-C, in which the results from initial a-C are also given for comparison. (A colour version of this figure can be viewed online.)

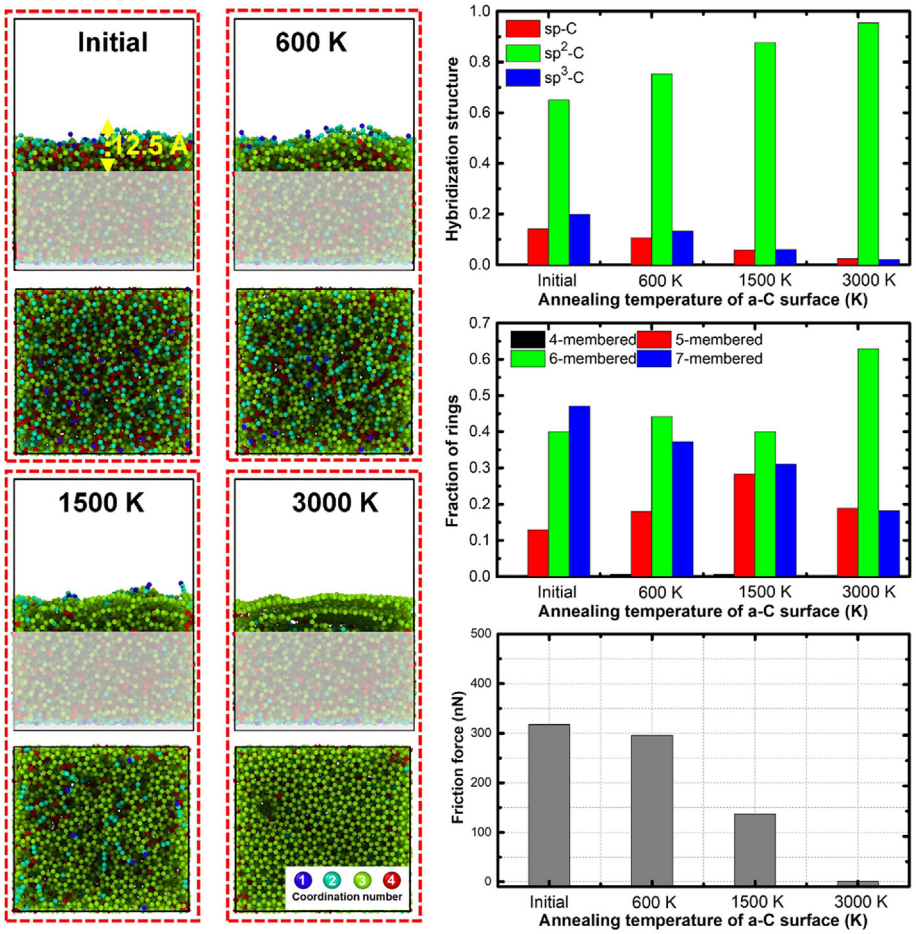

Fig. 7. Morphologies, hybridization, and fraction of rings of a-C films with different graphitized degrees, which are fabricated by annealing treatment under different temperatures (600, 1500, and 3000 K), are corresponding friction result. (A colour version of this figure can be viewed online.)

4. Conclusions

In this work, we fabricated different self-mated a-C friction systems with the graphitized structure and/or passivated surface, and comparatively explored the fundamental characteristics of graphitization and passivation mechanisms for low-friction behavior of a-C film by RMD simulation. By the systematical analysis of friction force, contact area, shearing strength, morphologies, and the interfacial nanostructure evolution, results revealed that.

- For the passivation mechanism, the chemical termination or rehybridization of dangling bonds of a-C surface could reduce both the real contact area and shearing strength of sliding interface, causing the reduction of friction force.
- However, for the graphitization mechanism, the low-friction property was highly dependent on the formed graphitized structure including size and layer number and the passivated state of a-C surface. When there were excessive dangling bonds of a-C surface, they interacted with the initial graphitized structure in the form of covalent bonds and thus the tribo-induced shearing effect caused the dissociation of graphitized structure.
- As the surface area of existed graphitized structure was smaller than the real contact area of friction interface in pure a-C system, it had no positive effect on the anti-friction behavior of a-C, and the low-friction mechanism was dominated by the passivation of a-C sliding interface. However, with increasing the size and layer number of graphitized structure, the sliding interface changed from a-C/a-C to a-C/G and G/G, reduced the shearing strength obviously, and thus resulted in the underlying explanation for low friction transited from the passivation-dominated, the synergistic effect between the passivation and graphitization to the graphitization-dominated mechanism.
- The present results disclose the fundamental difference of two popular low-friction mechanisms which is not accessible for an experimental approach, so it can be expanded as theoretical knowledge to account for the experimental phenomenon accurately and most importantly develop the new unidentified structures and technologies for anti-friction applications.

CRediT authorship contribution statement

Xiaowei Li: Conceptualization, Methodology, Software, Validation, Investigation, Writing - original draft, Writing - original draft, Writing - review & editing, Funding acquisition. **Aiying Wang:** Conceptualization, Writing - review & editing, Funding acquisition. **Kwang-Ryeol Lee:** Conceptualization, Methodology, Resources, Investigation, Writing - review & editing, Supervision, Funding acquisition.

Declaration of competing interest

The authors declare that they have no known competing financial interests or personal relationships that could have appeared to influence the work reported in this paper.

Acknowledgments

This research was supported by the Korea Research Fellowship Program funded by the Ministry of Science and ICT through the National Research Foundation of Korea (2017H1D3A1A01055070), the Nano Materials Research Program through the Ministry of Science and IT Technology (NRF-2016M3A7B4025402), and the National Natural Science Foundation of China (51772307).

Appendix A. Supplementary data

Supplementary data to this article can be found online at https://doi.org/10.1016/j.carbon.2020.08.014.

References

[1] J. Robertson, Diamond-like amorphous carbon, Mater. Sci. Eng. R Rep. 37 (2002) 129–281.
[2] Y. Wang, K. Gao, B. Zhang, Q. Wang, J. Zhang, Structure effects of sp^2-rich carbon films under super-low friction contact, Carbon 137 (2018) 49–56.
[3] K. Bewilogua, D. Hofmann, History of diamond-like carbon films-From first experiments to worldwide applications, Surf. Coating. Technol. 242 (2014) 214–225.
[4] S. Wan, D. Li, G. Zhang, A.K. Tieu, B. Zhang, Comparison of the scuffing behavior and wear resistance of candidate engineered coatings for automotive piston rings, Tribol. Int. 106 (2017) 10–22.
[5] C.A. Griffiths, S.S. Dimov, A. Rees, O. Dellea, J. Gavillet, F. Lacan, et al., A novel texturing of micro injection moulding tools by applying an amorphous hydrogenated carbon coating, Surf. Coating. Technol. 235 (2013) 1–9.
[6] R.K. Roy, K.R. Lee, Biomedical applications of diamond-like carbon coatings: a review, J. Biomed. Mater. Res. B 83B (2007) 72–84.
[7] F. Mangolini, B.A. Krick, T.D.B. Jacobs, S.R. Khanal, F. Streller, J.B. McClimon, et al., Effect of silicon and oxygen dopants on the stability of hydrogenated amorphous carbon under harsh environmental conditions, Carbon 130 (2018) 127–136.
[8] C. Donnet, A. Erdemir, Tribology of Diamond-like Carbon Films: Applications and Future Trends in DLC's Tribology, Springer, New York, 2007.
[9] K. Sun, X. Fan, W. Zhang, P. Xue, D. Diao, Contact-focusing electron flow induced nanosized graphene sheets formation in amorphous carbon film for fast low-friction, Carbon 149 (2019) 45–54.
[10] T.B. Ma, Y.Z. Hu, H. Wang, Molecular dynamics simulation of shear-induced graphitization of amorphous carbon films, Carbon 47 (2009) 1953–1957.
[11] Y.N. Chen, T.B. Ma, Z. Chen, Y.Z. Hu, H. Wang, Combined effects of structural transformation and hydrogen passivation on the friction behaviors of hydrogenated amorphous carbon films, J. Phys. Chem. C 119 (2015) 16148–16155.
[12] B. Lei, L. He, M. Yi, L. Ran, H. Xu, Y. Ge, et al., New insights into the microstructure of the friction surface layer of C/C Composites, Carbon 49 (2011) 4554–4562.
[13] H.A. Tasdemir, M. Wakayama, T. Tokoroyama, H. Kousaka, N. Umehara, Y. Mabuchi, et al., Wear behaviour of tetrahedral amorphous diamond-like carbon (ta-C DLC) in additive containing lubricants, Wear 307 (2013) 1–9.
[14] A.R. Konicek, D.S. Grierson, A.V. Sumant, T.A. Friedmann, J.P. Sullivan, P.U.P.A. Gilbert, et al., Influence of surface passivation on the friction and wear behavior of ultra nanocrystalline diamond and tetrahedral amorphous carbon thin films, Phys. Rev. B 85 (2012) 155448.
[15] X. Chen, C. Zhang, T. Kato, X. Yang, S. Wu, R. Wang, et al., Evolution of tribo-induced interfacial nanostructures governing superlubricity in a-C:H and a-C:H:Si films, Nat. Commun. 8 (2017) 1675.
[16] L. Cui, Z. Lu, L. Wang, Probing the low-friction mechanism of diamond-like carbon by varying of sliding velocity and vacuum pressure, Carbon 66 (2014) 259–266.
[17] J.D. Schall, G. Gao, J.A. Harrison, Effects of adhesion and transfer film formation on the tribology of self-mated DLC contacts, J. Phys. Chem. C 114 (2010) 5321–5330.
[18] T. Kuwahara, G. Moras, M. Moseler, Friction regimes of water-lubricated diamond (111): role of interfacial ether groups and tribo-induced aromatic surface reconstructions, Phys. Rev. Lett. 119 (2017), 096101.
[19] X. Li, A. Wang, K.R. Lee, Mechanism of contact pressure-induced friction at the amorphous carbon/alpha olefin interface, npj Comput Mater 4 (2018) 53.
[20] G.T. Gao, P.T. Mikulskl, J.A. Harrison, Molecular-scale tribology of amorphous carbon coatings: effect of film thickness, adhesion, and long-range interactions, J. Am. Chem. Soc. 124 (2002) 7202–7209.
[21] D.W. Kim, K.W. Kim, Effects of sliding velocity and normal load on friction and wear characteristics of multi-layered diamond-like carbon (DLC) coating prepared by reactive sputtering, Wear 297 (2013) 722–730.
[22] J. Huang, L. Wang, B. Liu, S. Wan, Q. Xue, In vitro evaluation of the tribological response of Mo-doped graphite-like carbon film in different biological media, ACS Appl. Mater. Interfaces 7 (2015) 2772–2783.
[23] S. Plimpton, Fast parallel algorithms for short-range molecular dynamics, J. Comp. Physiol. 117 (1995) 1–19.
[24] X. Li, P. Ke, H. Zheng, A. Wang, Structure properties and growth evolution of diamond-like carbon films with different incident energies: a molecular dynamics study, Appl. Surf. Sci. 273 (2013) 670–675.
[25] X. Li, A. Wang, K.R. Lee, Atomistic understanding on friction behavior of amorphous carbon films induced by surface hydrogenated modification, Tribol. Int. 136 (2019) 446–454.
[26] H.J.C. Berendsen, J.P.M. Postma, W.F. van Gunsteren, A. DiNola, J.R. Haak, Molecular dynamics with coupling to an external bath, J. Chem. Phys. 81 (1984) 3684–3690.
[27] F. Tavazza, T.P. Senftle, C. Zou, C.A. Becker, A.C.T. Van Duin, Molecular dynamics investigation of the effects of tip-substrate interactions during nanoindentation, J. Phys. Chem. C 119 (2015) 13580–13589.
[28] X. Li, A. Wang, K.R. Lee, Tribo-induced structural transformation and lubricant dissociation at amorphous carbon-alpha olefin interface, Adv Theory Simul 2 (2019) 1800157.
[29] X. Li, A. Wang, K.R. Lee, Insights on low-friction mechanism of amorphous carbon films from reactive molecular dynamics study, Tribol. Int. 131 (2019) 567–578.
[30] T. Kuwahara, P.A. Romero, S. Makowski, V. Weihnacht, G. Moras, M. Moseler, Mechano-chemical decomposition of organic friction modifiers with multiple reactive centers induces superlubricity of ta-C, Nat. Commun. 10 (2019) 151.
[31] S. Bai, H. Murabayashi, Y. Kobayashi, Y. Higuchi, N. Ozawa, K. Adachi, et al., Tight-binding quantum chemical molecular dynamics simulations of the low friction mechanism of fluorine-terminated diamond-like carbon films, RSC Adv. 4 (2014) 33739–33748.
[32] A. Erdemir, The role of hydrogen in tribological properties of diamond-like carbon films, Surf. Coating. Technol. 146–147 (2001) 292–297.
[33] A. Erdemir, Genesis of superflow friction and wear in diamond like carbon films, Tribol. Int. 37 (2004) 1005–1012.
[34] E. Rabinowicz, Friction and Wear of Materials, second ed., John Wiley & Sons, New York, 1995.
[35] T. Kunze, M. Posselt, S. Gemming, G. Seifert, A.R. Konicek, R.W. Carpick, L. Pastewka, M. Moseler, Wear, plasticity, and rehybridization in tetrahedral amorphous carbon, Tribol. Lett. 53 (2014) 119–126.
[36] S. Bai, T. Onodera, R. Nagumo, R. Miura, A. Suzuki, H. Tsuboi, et al., Friction reduction mechanism of hydrogen- and fluorine-terminated diamond-like carbon films investigated by molecular dynamics and quantum chemical calculation, J. Phys. Chem. C 116 (2012) 12559–12565.
[37] G.T. Gao, P.T. Mikulski, G.M. Chateauneuf, J.A. Harrison, The effects of films structure and surface hydrogen on the properties of amorphous carbon films, J. Phys. Chem. B 107 (2003) 11082–11090.
[38] Y. Liu, A. Erdemir, E.I. Meletis, An investigation of the relationship between graphitization and frictional behavior of DLC coatings, Surf. Coating. Technol. 86–87 (1996) 564–568.
[39] Y. Liu, E.I. Meletis, Evidence of graphitization of diamond-like carbon films during sliding wear, J. Mater. Sci. 32 (1997) 3491–3495.
[40] X. Li, X. Xu, Y. Zhou, K.R. Lee, A. Wang, Insights into friction dependence of carbon nanoparticles as oil-based lubricant additive at amorphous carbon interface, Carbon 150 (2019) 465–474.
[41] T. Luo, X. Chen, P. Li, P. Wang, C. Li, B. Cao, et al., Laser irradiation-induced laminated graphene/MoS2 composites with synergistically improved tribological properties, Nanotechnology 29 (2018) 265704.
[42] J. Li, C. Zhang, L. Ma, Y. Liu, J. Luo, Superlubricity achieved with mixtures of acids and glycerol, Langmuir 29 (2013) 271–275.
[43] J. Li, C. Zhang, L. Sun, X. Lu, J. Luo, Tribochemistry and superlubricity induced by hydrogen ions, Langmuir 28 (2012) 15816–15823.
[44] Y. Mo, K.T. Turner, I. Szlufarska, Friction laws at the nanoscale, Nature 457 (2009) 1116–1119.